

Journal of Materials Chemistry A

Accepted Manuscript

This article can be cited before page numbers have been issued, to do this please use: H. Zhang, Q. Gao, K. Yang, Y. Tan, W. Tian, L. Zhu, Z. Li and C. Yang, J. Mater. Chem. A, 2015, DOI: 10.1039/C5TA06668A.



This is an *Accepted Manuscript*, which has been through the Royal Society of Chemistry peer review process and has been accepted for publication.

Accepted Manuscripts are published online shortly after acceptance, before technical editing, formatting and proof reading. Using this free service, authors can make their results available to the community, in citable form, before we publish the edited article. We will replace this Accepted Manuscript with the edited and formatted Advance Article as soon as it is available.

You can find more information about *Accepted Manuscripts* in the **Information for Authors**.

Please note that technical editing may introduce minor changes to the text and/or graphics, which may alter content. The journal's standard <u>Terms & Conditions</u> and the <u>Ethical guidelines</u> still apply. In no event shall the Royal Society of Chemistry be held responsible for any errors or omissions in this *Accepted Manuscript* or any consequences arising from the use of any information it contains.



Published on 06 October 2015. Downloaded by ECOLE POLYTECHNIC FED DE LAUSANNE on 06/10/2015 14:14:49

DOI: 10.1039/C5TA06668A



Journal Name

COMMUNICATION

Solvothermal-induced α-Fe₂O₃/Graphene Nanocomposite with **Ultrahigh Capacitance and Excellent Rate Capability for** Supercapacitor

Received 00th January 20xx, Accepted 00th January 20xx

DOI: 10.1039/x0xx00000x

Hang Zhang, Qiuming Gao,* Kai Yang, Yanli Tan, Weiqian Tian, Lihua Zhu, Zeyu Li, and Chunxiao

Well crystallized Fe₂O₃ with the particle size mainly concentrated around 35-40 nm combined with graphene are fabricated under solvothermal condition. The optimized Fe₂O₃/GH-2 composite sample possessing of 49.7 wt% Fe₂O₃ has a high specific BET surface area of 215.3 m² g⁻¹. When served as supercapacitor electrode, the capacitances are admirable 2310 F g⁻¹ at 5 mV s⁻¹ and 615 F g⁻¹ at the amazing high current density of 100 A g⁻¹. Used as anode material of asymmetric hybrid capacitors, the composite shows promising future for energy storage with high energy density, high powder density and excellent cycle life.

Introduction

Supercapacitors, as a new kind of energy storage devices, possess excellent properties such as high power density, fast charge and discharge performances under large current density and long cycle life, especially compared to secondary batteries; however, the relatively low energy density based on the carbon electrode materials limits their general applications as the next generation power devices. To break through this obstacle, increasing the specific capacitance of the electrode material is regarded as an alternative route to enhance the energy density.^{2, 3} As to the special capacitance, the electrode active material plays a crucial role. There are two types of energy storage mechanisms for supercapacitors: one is the electrochemical double-layer capacitor, which is mainly applied for the carbon materials, and the other one is

pseudocapacitor occurred for the conductive polymers or transitional metal compounds because those kinds of materials may provide a variety of redox states for the reversible Faradic reactions. 4-7 In terms of the pseudocapacitor electrodes, transition metal compounds have attracted significant research attentions recently and different kinds of transition metal oxides have been studied as anode or cathode materials, such as MnO_2 , 8,9 Fe_3O_4 , 10 NiO, 5,11 CoO, 12 as well as multi-element transition metal oxides, e.g., NiCo₂O₄. ^{13, 14} Fe₂O₃ has been proved to be an alternative anode material based on its highly chemical and thermodynamical stable structure, ideal theoretical specific capacitance, low toxicity and natural abundance. 15-17 Nevertheless, it still suffers from the unsatisfactory ionic and electronic transport speeds, which lead to an insufficient utilization of active materials especially at large current density.

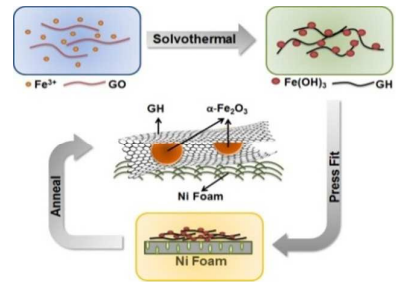
Unique designed nanostructure may provide short transfer distances and sufficient contacts between the transition metal oxide and electrolyte. Solvothermal technique has been convinced to be effective to obtain uniform Fe₂O₃ nanoparticles with excellent electrochemical properties. 18 In order to improve the conductive property of the materials and prevent the aggregation of nanosized transition metal oxides, graphene, a unique two-dimensional layered carbon material, has caused abundant interests for application to construct nanocomposites with transition metal oxides used as electrode materials due to their excellent electrical conductivities, high specific areas and outstanding structure stabilities. 2, 19-21 The

Key Laboratory of Bio-inspired Smart Interfacial Science and Technology of Ministry of Education, Beijing Key Laboratory of Bio-inspired Energy Materials and Devices, School of Chemistry and Environment, Beihang University, Beijing, 100191, P. R.

China. E-mail: qmgao@buaa.edu.cn; Fax:/Tel: +861082338212.

Electronic Supplementary Information (ESI) available: CV curves of Fe₂O₃/GH-1 and -3 at different scan rates, CV curves and TEM image of Fe $_2$ O $_3$ /GH-2 after 5000 cycles, CV curves of Fe₂O₃/GH-2 and GH at 20 mV s⁻¹, CV curves and galvanostatic charge-discharge curves of the $Fe_2O_3/GH//GH$ ASCs under different voltage windows, CV curves of the $Fe_2O_3/GH//GH\text{-II}$, -III and -IV ASCs, the special capacitance of different ASCs corresponding to different scan rates, galvanostatic charge-discharge curves of the Fe₂O₃/GH//GH-III ASC at different current densities, the special capacitance of the Fe₂O₃/GH//GH-III ASC tested at 5 A g⁻¹, the EIS analyses of the Fe₂O₃/GH//GH-III ASC before and after 5000 cycles test, CV curves of Ni foam loaded with and without Fe₂O₃/GH-2 at 20 mV s⁻¹ as well as the specific capacitance of Ni foam calculated by CV test. See DOI: 10.1039/x0xx00000x

Scheme 1 The formation process of α -Fe₂O₃/GH composite electrodes and mechanism illustrate of the electrode process.



DOI: 10.1039/C5TA06668A

COMMUNICATION Journal Name

graphene and transition metal oxide composite materials show fantastic improvements for the energy storage properties compared to single transition metal oxide materials, attributing to the novel designed nanostructures and the synergistic effects. 22, 23

In the past few years, there were some reports focusing on the Fe₂O₃ and graphene composites as supercapacitor electrode materials. 24-29 Wang et al. synthesized singlecrystalline Fe₂O₃/graphene composite via hydrothermal treatment with FeCl₃ and graphene as the precursors.²⁴ The Fe₂O₃ nanoparticles with size distributions between 50-200 nm were grown directly on the graphene hydrogels, which possess abundant three-dimensionally (3D) interconnected pores in the structures. A high specific capacitance of 908 F g⁻¹ was obtained at current density of 2 A g-1, benefitted by the combination of Fe₂O₃ and graphene. But the employ of conductive agent and binder would undisputedly increase the mass of electrode, resulting in some loss of capacitance. In addition, a uniform size distribution of the nanoparticles may lead to a good performance. The application of Fe₂O₃ on conductive carbon matrix as asymmetric supercapacitor (ASC) electrode material was reported. 16, 30, 31 Yang et al. studied on the solid-state ASC based on the MnO₂ nanowires and Fe₂O₃ nanotubes.31 Amorphous Fe₂O₃ nanotubes grown on the carbon fabric were fabricated using sacrificial template method. The hollow nanoarray was convenient for electrolyte contact and fast ionic transport. The energy density arrived at 0.55 mWh cm⁻³. However, more satisfied results would be realized if the more rational design of the Fe_2O_3 and carbon composite could be realized.

Experimental Methods

Published on 06 October 2015. Downloaded by ECOLE POLYTECHNIC FED DE LAUSANNE on 06/10/2015 14:14:49,

Syntheses of α-Fe₂O₃/Graphene Nanocomposite

Graphite oxide (GO) was synthesized from natural graphite powders by a modified Hummers method.³² In a typical preparation for the Fe₂O₃/graphene composite, first FeCl₃ solution (3 mL) was dropped into 50 mL GO solution (2 mg mL⁻¹). A sonication treatment was processed at 40 kHz for 2 h. Then, it was heated to 80°C and stirred for 30 min. The resulting product was gotten via centrifugation and redispersed into 50 mL dimethyl formamide (DMF) following by heat-treated at 180°C for 12 h. At last, the obtained black gel was washed with distilled water and ethanol, which was then cut into thin piece by knife, pressed onto Ni foam electrode. After vacuum dried, the electrode was annealed at 400°C for 2 h in Ar. For changing the weight ratio of Fe₂O₃ to graphene, the concentration of GO solution was varied (3, 2 and 1 mg mL⁻¹) while kept the volume constant. And the sample was noted as Fe₂O₃/GH-1, Fe₂O₃/GH-2 and Fe₂O₃/GH-3, respectively. The reduced graphene oxide hydrogel (noted as GH) was prepared by hydrothermally treatment of GO solution (2 mg mL⁻¹) at 180°C for 12 h. Subsequently the production was treated the same as what was mentioned above without the anneal procedure. The mass of active material on electrode was obtained by weighting the electrode before load

and after heat or dry treatment. For sample Fe₂O₃/GH-2, the average mass loaded on electrode is about 1 mg.

Materials Characterization

The samples were characterized by scanning electron microscope (SEM; Quanta-250 FEG, Holland), and high resolution transmission electron microscope (HRTEM; JEOL JEM-2100F). The crystalline structure of the samples were determinated on X-ray diffraction (XRD; Labx XRD-6000, Shimadzu, Japan) with Cu K_{α} radiation ($\lambda = 1.5418 \text{ Å}$). The scan rate was 3° min⁻¹ in the range of $10^{\circ} \le 2\theta \le 70^{\circ}$. N₂ sorption isotherms at 77 K were obtained on a Micromeritics ASAP 2020, with a degasification treatment at 300°C for 12 h. The special surface areas were calculated by the Brunauer-Emmett-Teller (BET) method and pore size distribution analyses were processed by the density functional theory (DFT) techniques. Raman spectra were obtained on a Lab RAM HR800 Raman spectrometer with the laser wavelength λ = 514 nm. Thermal gravimetric analyses (TGA) were carried out in air at a heating rate of 10°C min⁻¹ at a SDTQ600 (TA Instruments, USA) from room temperature to 700° C.

Electrochemical Measurements

The working electrodes were used directly after annealed or vacuum dried without any addition of conductive agents or binder. The electrochemical measurements in a threeelectrode system were carried out on a CHI660D electrochemical workstation with a platinum counter electrode and a Ag/AgCl reference electrode in 6 M KOH. While for the two-electrode test in CR 2025 coin cells, GH was used as the counter and reference electrodes, separated by a NKK porous fiber paper. The electrolyte was 6 M KOH aqueous solution. The related equations are listed as follows.³³

In the three-electrode measurement for CV curves, the special capacitance is calculated based on the equation: C = $S/(r \cdot m \cdot \Delta V)$, where C is the special capacitance, S is the absolute area of CV curve, and r, m and ΔV stands for the scan rate, mass of active material on the electrode and potential window corresponding to the CV curve, respectively. For the galvanostatic charge-discharge curves, the special capacitance is calculated as: $C = (I \cdot \Delta t)/(m \cdot \Delta V)$, where C is the special capacitance, I is the test current density, Δt and ΔV stands for the discharge time and the discharge potential window (not include of the voltage drop), and m is the mass of active material, respectively. As to the galvanostatic charge-discharge measurement of the ASC consisting of Fe₂O₃/GH and graphene, the equation is similar to the three-electrode system, but the m stands for the total mass of composite and graphene. Energy density (E) and power density (P) of the ASC could be calculated by the equations: $E = (1/2) \cdot (1/3.6) \cdot C \cdot V^2$; and $P = E/\Delta t$, where C is the special capacitance calculated before, V is the ASC voltage and Δt is the discharge time.

Results and Discussion

In this paper, Fe_2O_3/g raphene composite was prepared under solvothermal condition in DMF with subsequent anneal

Journal of Materials Chemistry A Accepted Manuscrip

Scheme 1. In solution, the Fe³⁺ ions were adsorbed on the surface of GO and uniformly distributed as a result of the electrostatic interaction, and finally transformed to α -Fe₂O₃ nanoparticles. The GH nanosheets reduced from GO were served as substrates for the α -Fe₂O₃ nanoparticles to grow. Meanwhile, driven by the π - π stacking interaction the GO nanosheets connected to each other at edges and selfassembled into the hydrogels with 3D networks.34 After pressed and annealed, the cavities in the 3D structure were partly contracted, leading to a hierarchically porous structure, which will be discussed later. And the heat treatment may help the graphene matrix to adhere onto the Ni foam, thus ensures a good electronic conduction of the electrode. confirmed by the XRD measurements. As shown in Figure 1a,

The crystal phases of the Fe₂O₃/GH composites can be the sharp diffraction peaks of α -Fe₂O₃ responding to the reflections of (012), (104), (110), (113), (024), (116), (018), (214) and (300) are all observed for the Fe₂O₃/GH-2 composite, suggesting a well crystallized hematite structure.³⁵ The broad reflection at $2\theta = 25.2^{\circ}$ (pointed out by the black arrow; corresponding to d-spacing of 3.54 Å) belongs to the (002) crystal planes of graphene. When compared to the diffraction peak of (002) crystal planes for GH occurred at $2\theta = 23.6^{\circ}$, meaning a d-spacing of 3.77 Å, the decrease of plane distances of graphene may be attributed to the anneal treatment and the interaction between $\alpha\text{-Fe}_2\text{O}_3$ and graphene nanosheets which promotes a slight restack. TGA measurements may confirm the accurate mass fractions of $\alpha\text{-Fe}_2\text{O}_3$ in the composites. Three curves (Figure 1b) all show rapid decrease from 400 to 500° C, as a result of graphene combustion in air. The α -Fe₂O₃ weight percent is 38.7%, 49.7% and 70.7% for Fe₂O₃/GH-1, Fe₂O₃/GH-2 and Fe₂O₃/GH-3, respectively.

Raman spectroscopy curves of the GH and Fe₂O₃/GH-2 samples are shown in Figure 1c and d. There are two main Raman bands at around 1347 and 1586 cm⁻¹ (Figure 1c). The former is related to the A_{1g} vibration mode of the disordered carbon (D-bond), while the later corresponds to the E_{2g} vibration mode of the ordered graphitic carbon (G-bond). The ratio of I_D/I_G comes to 0.98 and 1.01 respectively for the Fe₂O₃/GH and GH sample, meaning that the anchored Fe₂O₃ nanoparticles may hinder the partial reduction of GO by interaction of bridge oxygen. The characteristic peaks at 215, 277, 384, 454 and 587 cm⁻¹ could be clearly observed in Figure 1d severally corresponding to the A $_{g1}$ (1), E $_{g2}$ +E $_{g3}$, E $_{g4}$, A $_{g1}$ (2) and E_{g5} modes of Fe_2O_3 , which belong to the D_{3d}^6 crystal space group. $^{22,\,36}$ These results further confirm the hematite $\alpha\text{-Fe}_2\text{O}_3$ is successfully formed on the graphene matrix, which is consistent with the XRD results.

Typical type-IV curves were obtained from the N2 adsorption-desorption isotherms (Figure 1e), indicating the presence of mesoporous structures in all the composites. The textural parameters of three Fe₂O₃/GH composites are listed in Table 1. The specific surface area calculated by Brunauer-Emmertt-Teller (BET) method is 177.1, 215.3 and 103.1 m²g⁻¹ for Fe₂O₃/GH-1, Fe₂O₃/GH-2 and Fe₂O₃/GH-3, respectively. It can be concluded that the specific BET surface area is

remarkably influenced by the content of α -Fe₂O₃. The iron oxide nanoparticles anchored to graphene nanosheets would block some pores. On the contrary, the nanoparticles inlayed between graphene nanosheets could contribute to form new pores. The relationship between loaded contents of nanoparticles and pore size distributions is illustrated in Figure 1f. As to Fe₂O₃/GH-1, there are some mesopores and a certain amount of micropores with pore sizes around 1.2 nm retained because of incomplete blocking with a relatively low load of α - Fe_2O_3 . While for $Fe_2O_3/GH-3$, with a high load of α - Fe_2O_3 nanoparticles, it possesses mesopores with the largest average pore size of 15.4 nm. The Fe₂O₃/GH-2 presented a relatively concentrated small mesopores with the pore size distribution between 3 to 20 nm and an average pore size of 8.3 nm, which may be favorable for the impregnation of electrolyte through pore channel to realize efficient contact interface, ³⁷ suggesting the Fe₂O₃/GH-2 composite an excellent electrode material.

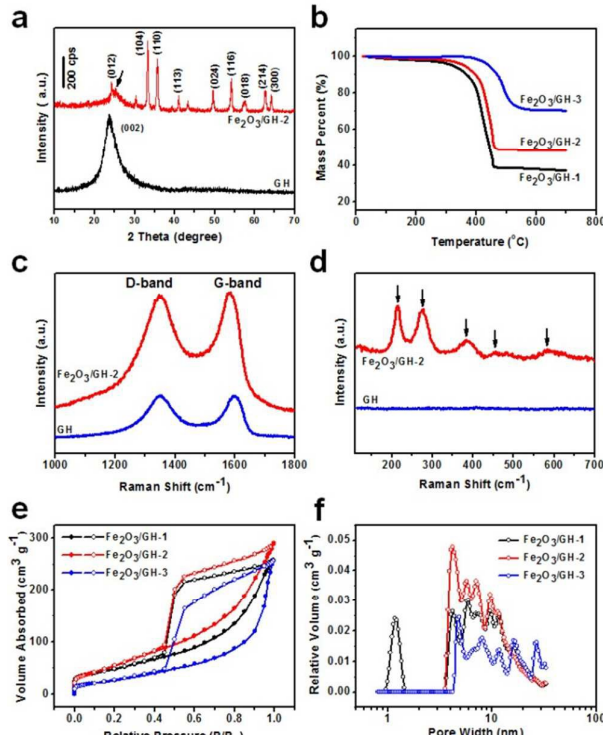


Figure 1. (a) XRD patterns of the Fe₂O₃/GH-2 composite and GH samples; (b) TGA curves of Fe₂O₃/GH-1, Fe₂O₃/GH-2 and Fe₂O₃/GH-3 composites; (c; d) Raman spectroscopy of Fe₂O₃/GH-2 composite and GH samples with the characteristic peaks of α-Fe₂O₃ signalled by the black arrows in (d); and N₂ sorption isotherms (e) and pore size distributions (f) of Fe₂O₃/GH-1, Fe₂O₃/GH-2 and Fe₂O₃/GH-3 composites.

Table 1. Textural parameters of the obtained three Fe₂O₃/GH samples.

-					
	Sample	$S_{BET} (m^2 g^{-1})^{a}$	$V_t (cm^3 g^{-1})^{b)}$	D _{DFT} (nm) ^{c)}	
	Fe ₂ O ₃ /GH-1	177.1	0.40	9.03	
	Fe₂O₃/GH-2	215.3	0.45	8.32	
_	Fe₂O₃/GH-3	103.1	0.40	15.42	

Spect represents the BET surface area; b) V_t represents the total pore volume; and c) D_{DET} stands for the DFT desorption average pore diameter.

Published on 06 October 2015. Downloaded by ECOLE POLYTECHNIC FED DE LAUSANNE on 06/10/2015 14:14:49,

DOI: 10.1039/C5TA06668A

Journal Name

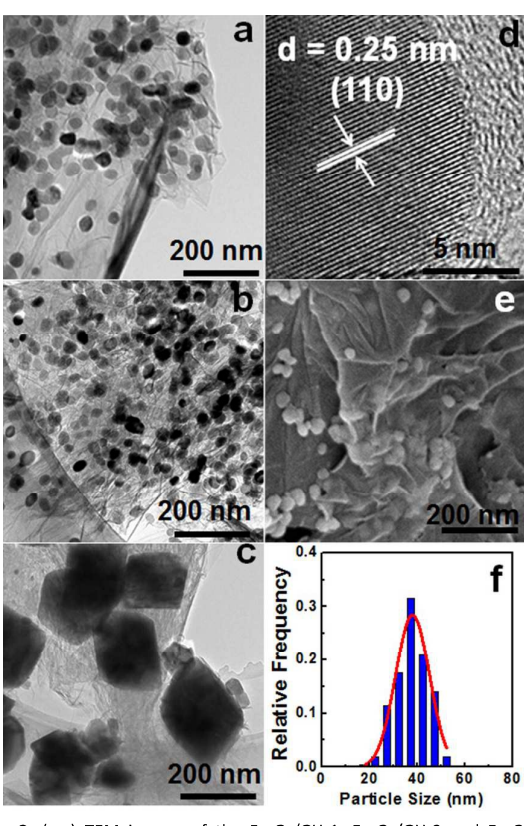


Figure 2. (a-c) TEM images of the Fe₂O₃/GH-1, Fe₂O₃/GH-2 and Fe₂O₃/GH-3 composites; HRTEM (d) and SEM (e) images of the Fe₂O₃/GH-2 composite; and (f) the particle size distribution of $\alpha\text{-Fe}_2\text{O}_3$ for the Fe $_2\text{O}_3$ /GH-2 composite.

TEM images were obtained to study the Fe₂O₃/GH composites. The graphene nanosheets with apparent wrinkles can be observed in all the samples (Figure 2a-c). When the mass ratios of $\alpha\text{-Fe}_2\text{O}_3$ are relative low for Fe $_2\text{O}_3$ /GH-1 and $Fe_2O_3/GH-2$, the spherical α - Fe_2O_3 nanoparticles are homogeneously anchored to the graphenes with uniform sizes less than 50 nm (Figure 2a and b). Enlarged HRTEM image of Fe₂O₃/GH-2 (Figure 2d) clearly indicates the high-quality crystalline character of α-Fe₂O₃. The measured distinct spacing of periodic lattice fringes is 0.25 nm, assigned to the interspacing of (110) planes of hematite α -Fe₂O₃, exactly matching with the XRD results. The distinct fringes owing to graphene are also obviously emerged, revealing that the graphene is gratifyingly reduced and partly crystallized after the solvothermal and anneal treatments. The contact interface is compact between the particle edge and graphene, demonstrating a tight combination of the two components. The surface morphologies of the Fe₂O₃/GH-2 sample were observed by SEM (Figure 2e). It can be clearly seen that most of α -Fe₂O₃ are clamped in the graphene layers while some α -Fe₂O₃ nanoparticles are anchored uniformly on the surface of crumpled graphene sheets, suggesting efficient assembly in the solvothermal progress and no obvious aggregation in the anneal treatment. Besides, the statistics of the nanoparticles size distribution for Fe₂O₃/GH-2 are processed and a standard normal distribution curve is shown in Figure 2f based on the

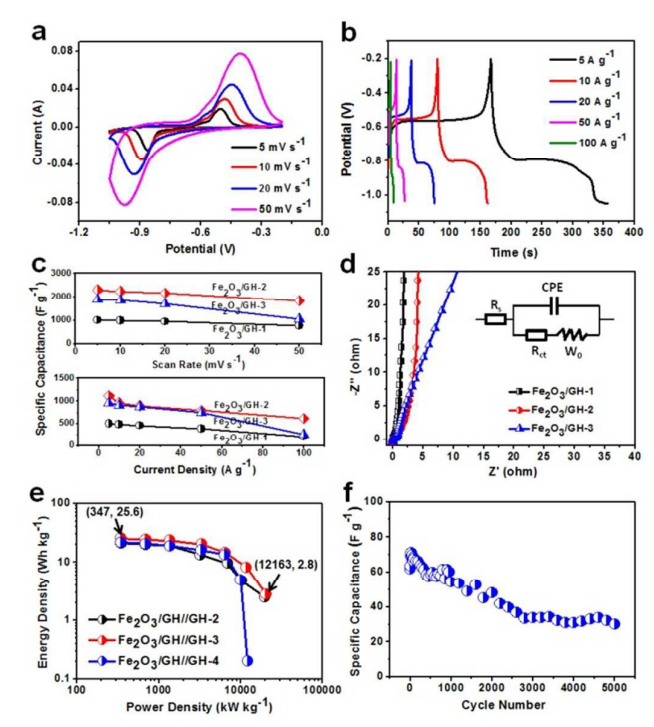


Figure 3. (a) CV curves at different scan rates, (b) galvanostatic charge-discharge curves at different current densities and (c) the special capacitances corresponding to the scan rates and current densities for the Fe₂O₃/GH-2 composite electrode; (d) the Nyquist plots of different Fe₂O₃/GH samples with the inset of the equivalent circuit: (e) the Ragone plot of the $Fe_2O_3/GH//GH-II$, $Fe_2O_3/GH//GH-III$ and $Fe_2O_3/GH//GH-IV$ ASCs; and (f) the cycle capacitance of Fe₂O₃/GH//GH-III ASC tested at current density

TEM image in Figure 2b. The particle size mainly concentrated around 35-40 nm with only as low as 5% smaller than 25 nm or larger than 50 nm, showing a homogeneous formation of the α -Fe₂O₃ nanospheres by the solvothermal method. With the weight percent rising to 70.7%, the α -Fe₂O₃ mostly existed in rhombic blocks with average size about 200 nm (Figure 2c), which would be disadvantageous for utilization of inner stuff. Some small spheres were formed, meaning uneven crystallization for Fe₂O₃/GH-3 composite.

When served as supercapacitor electrodes, electrochemical properties of the Fe₂O₃/GH-1, Fe₂O₃/GH-2 and Fe₂O₃/GH-3 samples are discussed in Figure 3. Typical CV curves of three samples with the potential window from -1.05 to -0.20 V versus Ag/AgCl at different scan rates are shown in Figure 3a and Figure S1a and b. The cathodic and anodic peaks are observed, corresponding to the reversible conversion between Fe3+ and Fe2+ ions. Even though the scan rate gets faster, the CV curves still preserve similar shape, suggesting an excellent rate capability. The specific capacitance of Fe₂O₃/GH-2 comes to admirable 2310 F g⁻¹ at 5 mV s⁻¹ and 1838 F g⁻¹ at 50 mV s⁻¹ (Figure 3c), the highest values over the Fe₂O₃ related materials (Table 2). While for the other two samples, the specific capacitance is 1018 and 1892 F g⁻¹ at 5 mV s⁻¹ for Fe₂O₃/GH-1 and Fe₂O₃/GH-3, respectively. The relatively unexpected storage value for Fe₂O₃/GH-1 may be caused by the low load of α -Fe₂O₃, while the insufficient utilization of Published on 06 October 2015. Downloaded by ECOLE POLYTECHNIC FED DE LAUSANNE on 06/10/2015 14:14:49,

DOI: 10.1039/C5TA06668A

COMMUNICATION

huge α -Fe₂O₃ particles should be responsible for the low

specific capacitance referred to Fe₂O₃/GH-3 sample. Galvanostatic charge-discharge test was introduced to evaluate the performance of the three composites. The resultant curves of Fe₂O₃/GH-2 at different current densities are shown in Figure 3b. The voltage platform at -0.80 V is associated with the convention from Fe3+ to Fe2+ ions. Meanwhile, the inverse process occurs at -0.55 V. 27 The special capacitances of the composites are also illustrated in Figure 3c. A capacitance of 1111 F g⁻¹ at 5 A g⁻¹ is obtained for Fe₂O₃/GH-2. Even if the current density is raised up to as high as 100 A g ¹, 615 F g⁻¹ can still be achieved, the highest values for iron oxide-based supercapacitor to the best of our knowledge (Table 2). This amazing result can be explained as follows. The synergistic effect of rational combination of α-Fe₂O₃ and graphene should be responsible for the high performance. The small and uniform size distribution of α -Fe₂O₃ nanoparticles ensures large contact interfaces with electrolyte and short ionic transport pathways and well-crystallized structure makes it much easy for electrons to conduct, thus guarantees the sufficient utilization of α -Fe₂O₃ even if at high current density. The interconnected graphene layers serve as "the highway" for electronic transports between the active material and electrode and also play as an effective storage container making full use of the large surface and numbers defect sites. The large numbers of mesopores can act as the temporary storage regions for electrolyte to supply ions when needed in the fast charge/discharge process.

The cycle life is another important factor for the supercapacitor materials. The $Fe_2O_3/GH-2$ sample electrode was tested at 20 mV s⁻¹ for 5000 cycles. The specific capacitances are shown in Figure S2. The capacitance retention is 46.8% with the maintained capacitance of 920 F g⁻¹, which is still larger than that of many other Fe_2O_3 related

materials. To vividly inflect the capacitance change, the CV curves of different cycles are shown in Figure S2b. The strength of feature peaks corresponding to convention between ${\rm Fe}^{2+}$ and ${\rm Fe}^{3+}$ decreased with the cycle processing, meaning that the capacitance fading is mainly caused by the inactivation of ${\rm Fe_2O_3}$. Partially damaged and aggregated ${\rm Fe_2O_3}$ nanoparticles could be observed on the TEM images (Figure S2c) for the ${\rm Fe_2O_3}/{\rm GH-2}$ after 5000 cycles due to the large surface energy of the small particle sizes which makes the nanoparticle unstable in a certain degree.

To further understand the electrochemical kinetics, the EIS spectra of the three samples were measured from 100 kHz to 0.01 Hz with the Nyquist plots given in Figure 3d. The intercept on the real axis of the Nyquist plots at high-frequency region is attributed to the resistance of the electrolyte (Rs). The semicircular pattern at middle-frequency is associated with the charge transfer resistance (Rct). The slope line at the low frequency region is due to the Warburg impedance (W₀) of ion diffusion and CPE is related to the constant phase element. 47 All the three samples possess very low values (about 0.5-1 Ω) for R_{ct}, due to the superior conductivity of graphene matrix. Besides, the abundant mesopores with large surface areas make it easy for electrolyte to immerse in and sufficiently contact with the electrode material. At the low frequency region, the more parallel to the imaginary axis of the line, the faster diffusion it can obtain. So it is obvious that the Fe₂O₃/GH-1 and Fe₂O₃/GH-2 composites showed more ideal ion diffusions, corresponding to the excellent supercapacitor performances especially at high current density.

Using the $Fe_2O_3/GH-2$ composite as anode and GH as the cathode, the ASCs with different mass ratios were assembled (Figure S3-5). A possible voltage of ASC can be around 1.4 V and the ideal mass ratio of $Fe_2O_3/GH-2$ to GH was chosen as 1:3 (denoted as $Fe_2O_3/GH//GH-III$). A capacitance of 176 F g⁻¹ is

 $\textbf{Table 2.} \ \textbf{Typical Fe}_2\textbf{O}_3 \ \textbf{related electrode materials and the electrochemical capacitance properties in aqueous electrolytes.}$

Electrode material	Electrolyte	Specific capacitance (F g ⁻¹)	Rate capability (F g ⁻¹)	Ref.
Porous α-Fe ₂ O ₃	0.5 M Na ₂ SO ₄	127 at 1 A g ⁻¹	40 at 14 A g ⁻¹	38
Porous α-Fe ₂ O ₃	0.5 M Na₂SO₄	193 at 1 A g ⁻¹	90 at 5 A g ⁻¹	39
Fe₂O₃/N-rGO hydrogel	1 M KOH	618 at 0.5 A g ⁻¹	350 at 10 A g ⁻¹	40
Graphene/Fe ₂ O ₃ nanorods	6 М КОН	320 at 10 mA cm ⁻²	152 at 100 mA cm ⁻²	41
Fe ₂ O ₃ films	1 M NaOH	178 at 5 mV s ⁻¹	121 at 100 mV s ⁻¹	42
Fe₂O₃/graphene	1 M Na ₂ SO ₄	226 at 1 A g ⁻¹	90.8 at 5 A g ⁻¹	43
Porous α-Fe₂O₃/graphene	1 M Na ₂ SO ₄	343.7 at 3 A g ⁻¹	182.1 at 10 A g ⁻¹	29
Graphene/Fe₂O₃/polyaniline	1 M KOH	638 at 1 mV s ⁻¹	-	44
N-rGO/Fe ₂ O ₃	1 M KOH	268.4 at 2 A g ⁻¹	137.0 at 5 A g ⁻¹	45
α -Fe ₂ O ₃ porous fibers	1 M LiOH	256 at 1 mV s ⁻¹	113.5 at 100 mV s ⁻¹	26
α-Fe₂O₃/graphene	1 M Na₂SO₄	306.9 at 3 A g ⁻¹	98.2 at 10 A g ⁻¹	46
Graphene/Fe₂O₃	1 M KOH	908 at 2 A g ⁻¹	622 at 50 A g ⁻¹	24
Fe ₂ O ₃ nanorod/graphene	1 M Na ₂ SO ₄	504 at 2 mA cm ⁻²	-	25
α-Fe₂O₃/graphene	6 М КОН	2310 at 5 mV s ⁻¹ 1111 at 5 A g ⁻¹	1838 at 50 mV s ⁻¹ 615 at 100 A g ⁻¹	Our wor

Journal Name

COMMUNICATION

obtained at 5 mV s⁻¹ from the CV measurements and the specific capacitance comes to 96 F g⁻¹ at 0.5 A g⁻¹ from the galvanostatic discharge capacitance examinations for the Fe₂O₃/GH//GH-III ASC. When the current density rises up to 50 A g⁻¹, 100 times larger, the ASC can still deliver a good capacity of 30 F g⁻¹ with retention of 31.3%. A high power density of 12,163 W kg⁻¹ can be delivered at the energy density of 2.8 Wh kg⁻¹ (Figure 3e). The highest energy density is 25.6 Wh kg⁻¹ achieved at the power density of 347 W kg⁻¹. The cycle life of the Fe₂O₃/GH//GH-III ASC was tested with the charge/discharge current density of 5 A g-1 for 5000 cycles (Figure 3f). The capacitance retention is 48.7%, showing good stability as a result of well combination of $\alpha\text{-Fe}_2\text{O}_3$ nanoparticles and graphene nanosheets in the composite. The decrease was mainly caused by the fading of the small Fe₂O₃ nanoparticles. The enlarged charge transfer resistance after 5000 cycles test (Figure S5c) also indicates that the partially destroyed and aggregated Fe₂O₃ nanoparticles make it harder for the electronic and ionic transports in the composite electrode, thus restrict the capacity.

Conclusions

Published on 06 October 2015. Downloaded by ECOLE POLYTECHNIC FED DE LAUSANNE on 06/10/2015 14:14:49

The Fe₂O₃/GH nanocomposite has been successfully fabricated through solvothermal method and subsequently anneal-treatment. The small homogeneous crystalline α-Fe₂O₃ nanoparticles guarantee a large amount of interfaces with electrolyte and enhance the utilization of active material, meanwhile the excellent combination of α -Fe₂O₃ and interconnected graphene sheets provides a fast electronic and ion transport, which make the Fe₂O₃/GH composite excitingly potential for fast energy storage. Ultrahigh capacitance and excellent rate capability could be gotten for the Fe₂O₃/GH-2 composite, indicating its amazing energy-power synergetic output characteristic.

Acknowledgement

This work was supported by National Basic Research Programs of China (973 Program, No. 2014CB931800), Chinese National Science Foundation (No. 21571010 and U0734002) and Chinese Aeronautic Project (No. 2013ZF51069).

Notes and references

1 M. Winter and R. J. Brodd, Chem. Rev., 2004, 104, 4245-

- B. G. Choi, M. Yang, W. H. Hong, J. W. Choi and Y. S. Huh, ACS Nano, 2012, 6, 4020-4028.
- Z. Li, Z. Xu, X. Tan, H. Wang, C. M. B. Holt, T. Stephenson, B. C. Olsen and D. Mitlin, Energy Environ. Sci., 2013, 6, 871-878.
- W. Tian, Q. Gao, Y. Tan, K. Yang, L. Zhu, C. Yang and H. Zhang, J. Mater. Chem. A, 2015, 3, 5656-5664.
- 5 Y. Tan, Q. Gao, W. Tian, Y. Zhang and J. Xu, Micropor. Mesopor. Mater., 2014, 200, 92-100.
- C. Feng, J. Zhang, Y. He, C. Zhong, W. Hu, L. Liu and Y. Deng, ACS Nano, 2015, 9, 1730-1739.
- J. M. D'Arcy, M. F. El-Kady, P. P. Khine, L. Zhang, S. H. Lee, N. R. Davis, D. S. Liu, M. T. Yeung, S. Y. Kim, C. L. Turner, A. T. Lech, P. T. Hammond and R. B. Kaner, ACS Nano, 2014, 8, 1500-1510.
- Z. Su, C. Yang, B. Xie, Z. Lin, Z. Zhang, J. Liu, B. Li, F. Kang and C. P. Wong, Energy Environ. Sci., 2014, 7, 2652-2659.
- G. Yu, L. Hu, M. Vosgueritchian, H. Wang, X. Xie, J. R. McDonough, X. Cui, Y. Cui and Z. Bao, Nano Lett., 2011, 11, 2905-2911.
- 10 M. Liu and J. Sun, J. Mater. Chem. A, 2014, 2, 12068-12074.
- 11 F. Luan, G. Wang, Y. Ling, X. Lu, H. Wang, Y. Tong, X.-X. Liu and Y. Li, Nanoscale, 2013, 5, 7984-7990.
- 12 C. Zhou, Y. Zhang, Y. Li and J. Liu, Nano Lett., 2013, 13, 2078-
- 13 C. Yuan, J. Li, L. Hou, X. Zhang, L. Shen and X. W. Lou, Adv. Funct. Mater., 2012, 22, 4592-4597.
- 14 G. Zhang and X. W. Lou, Adv. Mater., 2013, 25, 976-979.
- 15 K. Brezesinski, J. Haetge, J. Wang, S. Mascotto, C. Reitz, A. Rein, S. H. Tolbert, J. Perlich, B. Dunn and T. Brezesinski, Small, 2011, 7, 407-414.
- 16 S. Sun, J. Lang, R. Wang, L. Kong, X. Li and X. Yan, J. Mater. Chem. A, 2014, 2, 14550-14556.
- 17 L. F. Chen, Z. Y. Yu, X. Ma, Z. Y. Li and S. H. Yu, Nano Energy, 2014, 9, 345-354.
- 18 R. Wang, C. Xu, M. Du, J. Sun, L. Gao, P. Zhang, H. Yao and C. Lin, Small, 2014, 10, 2260-2269.
- 19 Y. Zhu, S. Murali, M. D. Stoller, K. J. Ganesh, W. Cai, P. J. Ferreira, A. Pirkle, R. M. Wallace, K. A. Cychosz, M. Thommes, D. Su, E. A. Stach and R. S. Ruoff, Science, 2011, 332, 1537-1541.
- 20 L. L. Zhang, X. Zhao, M. D. Stoller, Y. Zhu, H. Ji, S. Murali, Y. Wu, S. Perales, B. Clevenger and R. S. Ruoff, Nano Lett., 2012, 12, 1806-1812.
- 21 U. N. Maiti, J. Lim, K. E. Lee, W. J. Lee and S. O. Kim, Adv. Mater., 2014, 26, 615-619.
- 22 N. A. Kumar, H.-J. Choi, Y. R. Shin, D. W. Chang, L. Dai and J.-B. Baek, ACS Nano, 2012, 6, 1715-1723.
- 23 L. Peng, X. Peng, B. Liu, C. Wu, Y. Xie and G. Yu, Nano Lett., 2013, **13**, 2151-2157.

DOI: 10.1039/C5TA06668A

COMMUNICATION

Journal Name

Published on 06 October 2015. Downloaded by ECOLE POLYTECHNIC FED DE LAUSANNE on 06/10/2015 14:14:49,

24 H. Wang, Z. Xu, H. Yi, H. Wei, Z. Guo and X. Wang, *Nano Energy*, 2014, **7**, 86-96.

- 25 Q. X. Low and G. W. Ho, Nano Energy, 2014, 5, 28-35.
- 26 G. Binitha, M. S. Soumya, A. A. Madhavan, P. Praveen, A. Balakrishnan, K. R. V. Subramanian, M. V. Reddy, S. V. Nair, A. S. Nair and N. Sivakumar, J. Mater. Chem. A, 2013, 1, 11698-11704.
- 27 Q. Tang, W. Wang and G. Wang, J. Mater. Chem. A, 2015, 3, 6662-6670.
- 28 K. K. Lee, S. Deng, H. M. Fan, S. Mhaisalkar, H. R. Tan, E. S. Tok, K. P. Loh, W. S. Chin and C. H. Sow, *Nanoscale*, 2012, 4, 2958-2961.
- 29 S. Yang, X. Song, P. Zhang and L. Gao, *ACS Appl. Mater. Interf.*, 2015, **7**, 75-79.
- 30 H. Xia, C. Hong, B. Li, B. Zhao, Z. Lin, M. Zheng, S. V. Savilov and S. M. Aldoshin, *Adv. Funct. Mater.*, 2015, **25**, 627-635.
- 31 P. Yang, Y. Ding, Z. Lin, Z. Chen, Y. Li, P. Qiang, M. Ebrahimi, W. Mai, C. P. Wong and Z. L. Wang, *Nano Lett.*, 2014, 14, 731-736.
- 32 X. Zhu, Y. Zhu, S. Murali, M. D. Stoller and R. S. Ruoff, ACS Nano, 2011, 5, 3333-3338.
- 33 H. Wang, Z. Xu, A. Kohandehghan, Z. Li, K. Cui, X. Tan, T. J. Stephenson, C. K. King'ondu, C. M. B. Holt, B. C. Olsen, J. K. Tak, D. Harfield, A. O. Anyia and D. Mitlin, ACS Nano, 2013, 7, 5131-5141.
- 34 Y. Xu, K. Sheng, C. Li and G. Shi, *ACS Nano*, 2010, **4**, 4324-4330.

- 35 D. Maiti, V. Aravindan, S. Madhavi and P. Sujatha Devi, J. Power Sources, 2015, 276, 291-298.
- 36 D. L. A. de Faria, S. Venâncio Silva and M. T. de Oliveira, J. Raman Spectros., 1997, 28, 873-878.
- 37 S. Kondrat, C. R. Perez, V. Presser, Y. Gogotsi and A. A. Kornyshev, *Energy Environ. Sci.*, 2012, **5**, 6474-6479.
- 38 S. Shivakumara, T. R. Penki and N. Munichandraiah, ECS Electrochem. Lett., 2013, 2, A60-A62.
- 39 S. Shivakumara, T. Penki and N. Munichandraiah, *J. Solid State Electrochem.*, 2014, **18**, 1057-1066.
- 40 Z. Ma, X. Huang, S. Dou, J. Wu and S. Wang, *J. Phy. Chem. C*, 2014, **118**, 17231-17239.
- 41 W. Yang, Z. Gao, J. Wang, B. Wang and L. Liu, *Solid State Sciences*, 2013, **20**, 46-53.
- 42 P. M. Kulal, D. P. Dubal, C. D. Lokhande and V. J. Fulari, *J. Alloys Compd.*, 2011, **509**, 2567-2571.
- 43 Z. Wang, C. Ma, H. Wang, Z. Liu and Z. Hao, *J. Alloys Compd.*, 2013, **552**, 486-491.
- 44 X. Xia, Q. Hao, W. Lei, W. Wang, D. Sun and X. Wang, *J. Mater. Chem.*, 2012, **22**, 16844-16850.
- 45 H. D. Liu, J. L. Zhang, D. D. Xu, L. H. Huang, S. Z. Tan and W. J. Mai, J. Solid State Electrochem., 2015, 19, 135-144.
- 46 S. Yang, X. Song, P. Zhang, J. Sun and L. Gao, Small, 2014, 10, 2270-2279.
- 47 C. Yang, Q. Gao, W. Tian, Y. Tan, T. Zhang, K. Yang and L. Zhu, J. Mater. Chem. A, 2014, 2, 19975-19982.

